Journal of Biomedical Optics

BiomedicalOptics.SPIEDigitalLibrary.org

Toward microendoscopy-inspired cardiac optogenetics *in vivo*: technical overview and perspective

Aleksandra Klimas
Emilia Entcheva

SPIE.

Journal of Biomedical Optics 19(8), 080701 (August 2014)

OUTLOOK

Toward microendoscopy-inspired cardiac optogenetics *in vivo*: technical overview and perspective

Aleksandra Klimas[a] and Emilia Entcheva[a,b,c,*]
[a]Stony Brook University, Department of Biomedical Engineering, Stony Brook, New York 11794, United States
[b]Stony Brook University, Department of Physiology and Biophysics, Stony Brook, New York 11794, United States
[c]Stony Brook University, Institute for Molecular Cardiology, Stony Brook, New York 11794, United States

Abstract. The ability to perform precise, spatially localized actuation and measurements of electrical activity in the heart is crucial in understanding cardiac electrophysiology and devising new therapeutic solutions for control of cardiac arrhythmias. Current cardiac imaging techniques (i.e. optical mapping) employ voltage- or calcium-sensitive fluorescent dyes to visualize the electrical signal propagation through cardiac syncytium *in vitro* or *in situ* with very high-spatiotemporal resolution. The extension of optogenetics into the cardiac field, where cardiac tissue is genetically altered to express light-sensitive ion channels allowing electrical activity to be elicited or suppressed in a precise cell-specific way, has opened the possibility for all-optical interrogation of cardiac electrophysiology. *In vivo* application of cardiac optogenetics faces multiple challenges and necessitates suitable optical systems employing fiber optics to actuate and sense electrical signals. In this technical perspective, we present a compendium of clinically relevant access routes to different parts of the cardiac electrical conduction system based on currently employed catheter imaging systems and determine the quantitative size constraints for endoscopic cardiac optogenetics. We discuss the relevant technical advancements in microendoscopy, cardiac imaging, and optogenetics and outline the strategies for combining them to create a portable, miniaturized fiber-based system for all-optical interrogation of cardiac electrophysiology *in vivo*. [DOI: 10.1117/1.JBO.19.8.080701]

Keywords: cardiac optogenetics; microendoscopy; optical mapping.

Paper 140322KR received May 22, 2014; revised manuscript received Jul. 9, 2014; accepted for publication Jul. 17, 2014; published online Aug. 12, 2014.

1 Introduction

Disturbances in the electrical function of the heart, known as cardiac arrhythmias, are inherently complex spatiotemporal phenomena. Insights into cardiac activation, specific cell contributions to arrhythmogenesis, and cell-to-cell coupling abnormalities are essential for the development of future anti-arrhythmic therapies and for treatments of cardiac disease, in general. Such therapies include novel strategies for low-energy pacing and cardioversion,[1,2] as well as gene and cell delivery approaches for cardiac regeneration, and/or repair after myocardial infarction and in heart failure.[3,4] All these can benefit from improved methods for probing and imaging of the specific functional outcomes, e.g., quantifying the integration and contribution of transduced cells (upon gene therapy intervention, for example) to cardiac excitation patterns *in vivo*. In the last 20 years, a technique commonly known as optical mapping has become the norm for visualization of such electrical signals in heart tissue *in vitro* or *in situ* using voltage- or calcium-sensitive fluorescent dyes.[5–7] As technological advancements have brought about imaging devices with increasingly higher spatiotemporal resolution, there is a desire for complementarily more precise, spatially localized stimulation of specific cells or regions within the tissue, which is hard to achieve via electrical stimulation using traditional electrodes.

To overcome the resolution limits of electrical stimulation, a technique known as optogenetics has recently been developed, allowing for both targeted optical stimulation and optical sensing of cells by using genetic methods to yield cell-specific expression of light-sensitive ion channels and pumps.[8–11] In neuroscience, studies using optogenetics *in vivo* employing small-diameter optical systems have become standard practice. However, the recording of elicited brain responses is still primarily achieved by electrical means at a relatively low-spatial resolution.

Although optrodes have been used for optically recording excitation within the heart wall,[12–15] no system for recording at the endocardial surface has been developed to date, either for optical stimulation or for optical mapping, in whole hearts and *in vivo*. Optically imaging from outside dense heart tissue is fundamentally limited to the epicardial surface by photon scattering and absorption. Thus, specific components of interest lying close to the endocardial surface, such as the internal conduction system [e.g., the sinoatrial (SA) node, the atrioventricular (AV) node, and the Purkinje system (PS)], have remained out of reach for cardiac optical mapping in whole hearts. These conduction system structures are critical in understanding a wide class of rhythm disorders, as well as for the development of new pacing and cardioversion approaches. Furthermore, *in vivo* (endocardial) probing and imaging are the most direct ways to document the functional contribution

*Address all correspondence to: Emilia Entcheva, E-mail: emilia.entcheva@stonybrook.edu

0091-3286/2014/$25.00

of transduced cells in recent gene therapy strategies including transendocardial viral delivery[16] or cardiac stem cell therapy in nonhuman primates.[17] Newly developed fiber-optic microendoscopic probes have emerged in neuroscience, designed exclusively for *in vivo* optical recordings in the brain, including calcium imaging. These probes underlie miniaturized (Ø < 1 mm) optical systems that show promise for integration with cardiac catheterization techniques to optically access the endocardial surface of whole hearts and *in vivo* and potentially both stimulate and record from cells and structures of interest.

In this technical perspective, we outline the essential methods from cardiac imaging, optogenetics, and microendoscopy toward the design of miniaturized fiber-based probes for all-optical interrogation of cardiac activity *in vivo*. In particular, we show how these methods can be used to overcome some of the design challenges to produce an all fiber-optic based system, i.e., obtaining adequate access to internal structures, overcoming light penetration limits, accommodating multiple wavelengths for stimulation and recording, accounting for the limited emitted fluorescence from fast-responding voltage-sensitive dyes, and performing measurements with high-spatiotemporal resolution. Such a portable solution will allow probing deep within the heart to induce and/or map the activation of specific cell regions, which is not possible using current optical imaging techniques.

2 Optical Imaging in Cardiac Electrophysiology

The understanding of cardiac arrhythmias requires the knowledge of the underlying mechanisms of both local cell-level electrical activity as well as global syncytium-level propagation through cardiac tissue. Although electrode arrays can be used for multisite electrical recording, they are limited in spatial resolution and typically do not provide detailed information about cell repolarization and action potential maps, but report extracellular signals. Thus, fluorescent probes capable of relaying membrane potential and intracellular calcium concentration with high-temporal resolution are currently used to perform high-resolution measurements of electrical activity. When combined with newer high-speed, high-sensitivity cameras, simultaneous multisite optical recording of electrical signal propagation in cardiac tissues can be performed by optical mapping, extensively covered in other reviews.[5–7]

2.1 *Optical Mapping*

Accurate tracking of the propagation of electrical waves requires high-spatiotemporal resolution measurements—typically, signal acquisition rates of least 200 Hz and spatial resolutions at the cellular scale plus ample field of view (FOV).[6] Early cardiac optical measurements[18,19] followed in the footsteps of work on optical mapping of neuronal excitation *in vitro* and *in vivo*[20,21] at low spatial and temporal resolutions. Later, photodiode arrays (PDAs) were used to track the propagation of electrical disturbances in whole hearts;[22–24] but such measurements have limited spatial resolution. The development of high-speed cameras, such as charged coupled device (CCD) cameras and more recently electron multiplying CCD (EMCCD) cameras, has allowed the tracking of more intricate waveforms in tissues[25–27] and whole hearts.[28–35] Temporal resolutions can be increased without sacrificing spatial resolution by using methods such as temporal pixel multiplexing, where pixel exposure times are offset allowing temporal information to be embedded into the image without adjusting the intrinsic frame rate of the camera.[36] This method has been employed to perform 250-Hz Ca^{2+} imaging of rat cardiomyocytes using a 10-Hz megapixel CCD camera and a digital micromirror device to perform the transient illumination of subregions of the detector.[36]

Fluorescent mapping of electrical propagation within the heart tissue is limited to the tissue surface and subsurface by photon scattering and absorption. Additionally, recorded signals at larger depths can become distorted, as fluorescence imaging is depth integrated for two-dimensional imaging techniques such as optical mapping, making it hard to understand the three-dimensional (3-D) wave propagation in whole hearts. Larger penetration depths and improved signal qualities have been demonstrated in whole hearts[30,32–34] and heart slices[27,37–40] using near-infrared voltage-sensitive dyes; however, imaging depth still remains limited. Thus, optical recordings of important features of the conduction system, such as the PS lying close to the endocardial surface,[41] have remained unexplored in the intact heart due to the inadequacies of current imaging methods.

It is possible to perform 3-D mapping in tissue samples by employing optical transport models in combination with computational methods to reconstruct the electrical propagation in three dimensions. However, these methods require combining and processing images obtained from both sides of the tissue in order to estimate the source of electrical disturbances within the heart wall.[23,33,35,36] Because this method cannot be applied to whole hearts, optical tomography techniques have been used for depth-resolved imaging.[42] Although these imaging methods are less invasive compared with inserting probes directly into the tissue,[39] model-based reconstruction requires significant post-processing using complex algorithms and assumptions that do not account for structural, optical, or electrical heterogeneities within the tissue.[27,37–39]

2.2 *Optrodes in Cardiac Imaging*

Depth resolution limits due to photon scattering and absorption and motion artifacts have been mitigated using optical systems combining both optical fibers and electrodes—known as "optrodes." An example optical schematic of an optrode used in cardiac optical mapping can be seen in Fig. 1. Early fiber-based systems were integrated into existing fluorescent microscope setups to perform optical recordings without the need for heart preparations to be mounted on to the microscope as well as to minimize motion artifacts.[12,43,44] Simultaneous multisite intramural voltage and calcium measurements were then performed within the walls of Langendorff-perfused rabbit, pig, and canine hearts.[13,14,45–48] Such *ex vivo* recordings using optrode systems consisting of fiber bundles provide an alternative view of intramural activity and do not require complex computational methods to correct for signal distortions due to photon absorption and scattering. Although measurements using optrodes have been performed in blood-perfused pig hearts,[46] they have limited applications in behaving animals *in vivo*, as they require direct insertion into the heart wall.

3 Optical Actuation via Optogenetics

Electrical stimulation provides a relatively crude interrogation method of biological systems, as it is limited in spatial resolution by electric field effects and cannot target specific cell types. The emergence of optical means for stimulation, e.g., optogenetics—a term first coined by Deisseroth et al.[10]—provided a toolbox of microbial opsins (light-sensitive ion channels) to optically

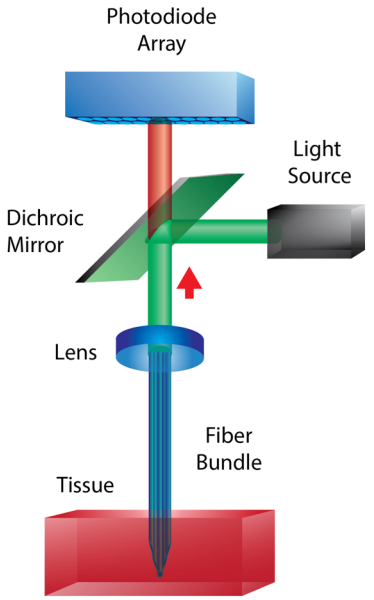

Fig. 1 Example of a fiber-optic imaging system for multisite optical recording of cardiac tissue. The fiber bundle consists of multimode fibers terminated at different lengths in order to Di-4-ANBDQBS. Collected light from the fiber bundle is either imaged onto a second fiber bundle connected to individual photodiodes to perform ratiometric measurements[13,49] or imaged directly on to a photodiode array (PDA).[14,47,48,50]

actuate genetically targeted cells with high-spatiotemporal resolution. Examples of these optical actuators can be seen in Table 1. The discovery, the characterization, and the application of the microbial opsins Channelrhodopsin-1 (ChR1) and Channelrhodopsin-2 (ChR2) to mammalian cells[8,9] were followed by the demonstration of the usefulness of these optogenetic tools in the study of neural circuits, as they provide millisecond timescale control of neuronal spiking, control of synaptic responses, trigger specific behaviors, and facilitate the mapping of neuronal circuits.[51–53] In addition to excitatory means of stimulation, hyperpolarizing channels such as the light-driven chloride pump Halorhodopsin (NpHR)[54,55] and the light-driven proton pump Archaerhodopsin-3 (Arch)[56] can be used to inhibit the cellular activity. For example, NpHR has been used in the optical control of idiopathic-induced epileptic seizures in freely behaving rats.[55] When combined with depolarizing channels, such as ChR2, these hyperpolarizing opsins allow for precise bidirectional cellular manipulation—either silencing or activation by light.[56] In addition, the development of opsin variants such as Chrimson and Chronos—a red-shifted ChR2 variant and a more light-sensitive, faster ChR2 variant, respectively—provides a means of targeting different neuronal populations within the same FOV.[57]

3.1 *Neural Optogenetics via Optical Fibers*

In vivo experiments in intact mammals have become standard practice for optogenetics in neuroscience. Early optogenetic manipulation of neural tissue *in vivo* was made possible by the use of fiber optics, where stimulation light can be delivered via one or more optical fibers with signal readout typically performed using electrodes. Although verification of optogenetic stimulation *in vivo* can be determined by recording behavioral responses from subjects,[58–61] electrical information is usually preferred in order to ensure proper targeting of the desired

Table 1 Examples of commonly used fluorescent indicators and actuators.

Commonly used optical indicators			
	Type	Ex (nm)	Em (nm)
Di-4-ANBDQBS	Voltage sensor	640	>700
Di-8-ANEPPS	Voltage sensor	530	620
Rhod-4	Calcium sensor	524	551
Fura-2	Calcium sensor	340/380	510
EYFP	Reporter	515	530
EGFP	Reporter	480	510
Genetically encoded optical indicators			
Arch-D95N	Voltage sensor	585	687
Arch-EEN	Voltage sensor	633	697
VSFP3 (mKate)	Voltage sensor	508	633
GCaMP	Calcium sensor	497	512
Genetically encoded optical actuators			
	Type	Ex (nm)	
ChR2	Depolarizing ion channel	470	
ArchT	Repolarizing proton pump	575	
NpHR	Repolarizing chloride pump	580	

neuronal populations. Early studies in freely behaving mice[56,62] and in awake macaques[63,64] employed single-optical fibers and recording electrodes, including electroencephalographic and electromyographic electrodes, and were used to measure electrical changes triggered by light in ChR2- or ArchT-expressing neurons.

Multipoint electrical readout of optical stimulation has been demonstrated using multielectrode optrodes and multichannel electrode arrays in behaving rodents[65,66] and in awake rhesus monkeys.[67] However, the subjects must be tethered to optical sources and recording systems using bulky optical fibers and cables. Some bulk can be reduced by directly coupling multiple light emitting diodes (LEDs) to optical fibers to allow for free movement,[68] but cables are still required for electrical readout. Permanently mounting the device to the subject can be avoided by employing optically clear windows, which can be penetrated by fine recording electrodes, and has been successfully demonstrated in rhesus monkeys.[69] These windows have the potential to be prone to infection[69] and cannot easily be applied to systems, such as the heart, which cannot be directly accessed from outside the body.

Similar to optical mapping, tissue penetration for optical stimulation is limited by photon scattering and absorption, particularly when using shorter-wavelength light-sensitive channels such as ChR2 (470 nm). For depth-resolved multipoint stimulation in behaving rodents, silicon-based probes with single or

multiple μm-scale optical waveguides have been used,[70,71] which are miniaturized analogs to the angle-polished fibers used in cardiac optical mapping. Their small size allows them to be easily used in an array and 3-D distributed, and when spatially scanned, can be used to perform independent multipoint stimulation.[72] Further miniaturization of these optrodes has been achieved using μLEDs directly mounted onto the silicon probe, where light is focused using photo-polymerized lenses surrounded by multiple recording electrodes.[73] However, all-optical actuation and sensing systems *in vivo* have yet to be developed. Systems using an injectable, flexible optrode system containing a microinorganic LED (μ-ILED; 6.45-μm thick, 50×50 μm^2), temperature sensor, and microinorganic photodiode (μ-IPD; 200×200 μm^2) have shown promise in freely moving mice expressing ChR2, but the μ-IPD was only used to measure the irradiance of stimulation light, rather than performing an optical readout.[74] Currently, these systems lack detectors with high enough sensitivities to sufficiently measure the fluorescence of currently available probes.

Two-photon activation can also be used to achieve larger actuation depths in tissue, without requiring insertable probes.[75] Although two-photon activation of ChR2 has been demonstrated to invoke the neuronal stimulation at depths up to 60 μm in mouse cortical slices,[76] large amounts of light are usually required for activation,[77] and systems typically involve some form of scanning mechanism. Scanless systems employing spectrally separated high-powered light pulses have demonstrated stimulation of ChR2-expressing neurons in rodent brain slices at depths greater than 200 μm;[78,79] but these high-energy methods may not be practical for use in behaving subjects.

Current studies in optogenetics in the brain rely on actuation and recording systems that cannot be easily translated to use in the heart. Head-mounted systems require removal of a section of the skull to access the brain. Straight, ridged optrodes can be used by taking advantage of the short distance between the skull and the brain, and the system does not need to be designed to travel through small diameter structures to access regions of interest in a minimally invasive manner.

3.2 *Emerging Cardiac Optogenetics*

Because the heart is a heterogeneous structure comprised of multiple cell types having different excitation thresholds, the ability to perform actuation of specific cell types—as enabled by optogenetics—can aid the understanding of their unique contributions to electrical disturbances leading to arrhythmias. More specifically, this will allow for better dissection of the roles of specific parts of the conduction system (e.g., the SA node, the AV node, and PS) by employing promoters for genes specifically expressed in the conduction system of the heart (e.g., HCN4 and Cx40).[11] Such cell-type specific actuation and sensing of electrical activity within the cardiac tissue *in vivo* have not yet been demonstrated; a key factor limiting expansion to *in vivo* applications has been the inability to optically access regions of interest inside the intact heart.

The application of optogenetics to the cardiac field is rather recent;[11] the first experiments were performed in transgenic zebrafish, where ChR2- and NpHR-transduced cardiomyocytes were used to track the origin of pacemaking.[80] Studies employing optogenetics in mammalian cardiac tissue first used ChR2-expressing transgenic mice.[81] In addition to transgenic animals and transdifferentiation of ChR2-expressing stem cells into cardiomyocytes,[82] current cardiac optogenetics studies[80–84] employ viral delivery using adenoviral vectors for ChR2 and ArchT in both neonatal and adult cardiomyocytes,[83,84] or use a cell delivery method, where nonexcitable cells expressing ChR2 are coupled to cardiomyocytes.[85] Furthermore, all-optical actuation and sensing has been demonstrated in conjunction with high-resolution optical mapping with neonatal rat cardiomyocytes using ChR2 for actuation simultaneously with Rhod-4 for calcium reporting.[85]

Experimental data have been used to develop computational models incorporating accurate representations of opsin channel kinetics,[83,86] spatial distribution of photosensitive cells, and tissue illumination constraints to determine the optimal targets for optogenetic stimulation in the whole heart.[41,87] For example, it has been computationally demonstrated that the optogenetic targeting of the PS, found close to the endocardial surface, could be used to optically perform cell-specific sinus-like pacing with lower energies compared with ventricular targets.[41] Although *in vivo* optical actuation has been demonstrated using open-chest procedures in mice,[81] current recording methods are limited to the epicardial surface and subsurface due to photon scattering and absorption, making specific mapping of the internal conduction system infeasible.

Unlike optogenetic stimulation in neuroscience, which can rely on rigid head-mounted systems for direct access to the brain, *in vivo* cardiac optogenetics requires new instrumentation. Optical interrogation from the endocardial surface would provide a means to directly access the conduction system, but would require the development of a small, flexible imaging system similar to those used in cardiac catheter-based imaging and in microendoscopy.

4 Endoscopic Imaging Systems

Microendoscopy was born out of the need for miniaturized, portable fluorescence microscope systems for performing high-resolution *in vivo* diagnostic imaging. With the advent of high-speed cameras and optical fibers, imaging optics can be separated from bulkier light sources and detectors. Newly developed miniaturized, high-NA gradient index (GRIN) objectives allow for even smaller diameter imaging systems compared with conventional imaging objectives, making it possible to navigate through small orifices for imaging, including in awake, freely moving subjects. Microendoscopy lends two key components of relevance to *in vivo* cardiac imaging: remote delivery using optical fibers and high resolution, miniature probes for imaging. Here, we outline some key aspects of microendoscopic imaging systems that could prove useful for *in vivo* cardiac optogenetic studies.

4.1 *Microendoscopy*

Microendoscope systems can employ single-optical fibers, fiber-optic imaging bundles (FOIBs), or free-space optics (i.e., no waveguides or optical fibers) to deliver light from lasers, arc lamps, and LEDs to tissue and in turn to collect reemitted light to photomultiplier tubes (PMTs), CCDs, or complementary metal-oxide semiconductor (CMOS) detectors. Early microendoscopic systems were developed to replicate larger, free-space confocal imaging systems and fluorescence microscopes. These probes were commonly constructed using microscope objectives or sets of aspheric lenses to couple light into a single- or multimode fibers or fiber bundles. Schematics of these systems are shown in Fig. 2. *In vivo* imaging requires probes with diameters

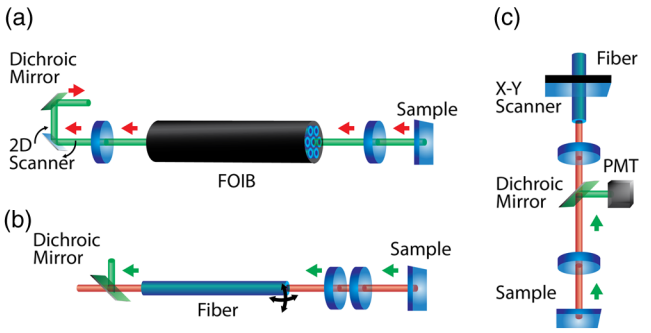

Fig. 2 Schematic of early microendoscopic imaging systems. (a) Fiber-optic imaging bundle (FOIB) system: Light is scanned across a FOIB using a two-dimensional (2-D) scanner and focused on to the sample using an objective to perform the single-photon confocal imaging.[91] (b) Compact two-photon imaging system: A probe containing a lens system scans light across a sample to perform the two-photon imaging *in vivo* and *in vitro*.[89,90,92] (c) Miniaturized microscope: Light from a single-mode fiber is scanned across a sample using a head-mounted unit containing a scanner, dichroic mirror, focusing lenses, and photomultiplier tube (PMT) to perform *in vivo* two-photon imaging.[88]

on the order of millimeters; thus, multiple lenses are needed to correct aberrations inherent to small diameter conventional optics. Head-mounted systems, similar to those used in optogenetic studies in the brain, have been used to perform the imaging of calcium transients in awake rats;[88] however, these systems typically provide only a modest light-gathering ability (<0.35 NA).[89,90]

4.2 *GRIN Lenses*

GRIN materials have a continuously varying index of refraction that causes the light to bend as it propagates through the material. GRIN rods can be used as efficient light guides in microendoscopy by confining light within the material. The length of the GRIN rod is given in terms of pitch, i.e., the number of periods the light has propagated. Whole-integer pitch rods have unitary magnification and are commonly used as relay lenses, whereas half-integer pitch rods similarly provide a non-magnified inverted image. Quarter-pitch GRIN rods are a special case, as they can be used as the focusing element to either image an object at infinity as a point source, or vice versa. If the GRIN lens has a length slightly less than a quarter-integer pitch, then they have a nonzero working distance (WD). Typically, the WD of the probe is designed based on the application and aberrations are minimized for imaging at that distance. Most GRIN optical systems can be seen as infinity-corrected microscope objectives that focus light on a specimen and collect emitted light, while a relay lens focuses emitted light onto collection optics such as optical fibers and objectives for the imaging system.[93] However, because of the inherent wavelength dependence of refractive materials, GRIN systems are prone to chromatic aberrations. These dispersion effects can be minimized by limiting the length of the GRIN elements[94,95] or by using dispersion-compensation elements such as grating-prism assemblies.[96]

4.3 *GRIN Microendoscopes*

The use of GRIN lenses has facilitated the design of smaller diameter, high-NA imaging systems to navigate within small structures (Fig. 3). They provide a cheaper alternative to conventional optics and require fewer optical elements to create a small diameter, high-NA imaging system. Having NAs as high as 0.65, with diameters from 350 μm to 2 mm and lengths up to 7.8 mm, they have proven to be effective imaging tools in miniaturized systems that require high-spatiotemporal resolution imaging both *in vivo* and *in vitro*.

Microendoscopes have been used to perform *in vitro* and *in vivo* high-resolution imaging of mouse brain tissues [Fig. 3(e)][96,103] and to obtain *in vivo* video-rate movies [Fig. 3(b)][94] and two-photon images [Fig. 3(a)][98] of cerebral blood flow in the brains of anesthetized mice. They can be easily integrated into compact, portable head-mounted assemblies; systems as small as 2.9 g have been used to image the blood flow and vasculature in anesthetized mice [Fig. 3(f)].[104,105] Of particular interest are head-mounted GRIN-based systems for *in vivo* functional imaging of neural activity as they demonstrate spatiotemporal resolutions of relevance for cardiac imaging. Examples include a system to image Ca^{2+} dynamics of cerebellar Purkinje cells in behaving mice with a head-mounted FOIB probe to couple the signal onto an EMCCD camera [Fig. 3(d)][102] and a compact, head-mounted system containing an LED light source and a CMOS detector [Fig. 3(b)].[99] Because of their large NA compared with their relatively small diameter, GRIN lenses are an ideal choice for *in vivo* applications, including imaging inside the heart. This provides the light-gathering ability necessary to make *in vivo* imaging and actuation and yields performance comparable with free-space optical systems.

5 In Vivo Cardiac Imaging by Endoscopic Routes

Cardiac catheterization is widely used clinically for structural imaging within the heart, performing electrical measurements as well as ablation therapies and other procedures for the treatment of arrhythmias. In clinical cardiac imaging (e.g., angioscopy, optical coherence tomography, and spectroscopy, as shown in Table 2), catheter-based fiber optic systems are used to perform real-time, high-resolution optical imaging for diagnostic procedures and surgery guidance inside the heart. To overcome photon scattering and absorption by blood, a distal balloon used to occlude the blood flow or optically clear fluid flushed in front of the optical fiber can be used to create a blood-free environment.[106–108] Furthermore, near-IR spectroscopy can be used with an intravascular ultrasound system to obtain simultaneous spectral and anatomical information through flowing blood.[108,109]

From such clinical catheterization studies, we summarize below the relevant information for endoscopic access routes into the human heart. Access to major vessels and cardiac chambers for cardiac catheterization is performed using percutaneous approaches, i.e., entering through femoral arteries (diameter 5.5 to 7.5 mm), femoral veins (diameter 9 to 14 mm at rest), internal jugular veins (diameter 11 to 22 mm), or through direct surgical exposure of the brachial vein (diameter ~4 mm).[108,111–114] Guide catheters used in intravascular imaging systems and coronary angioplasties have outer diameters between 6 and 9 Fr (3 Fr = 1 mm).[115,116] In cases where the AV node, SA node, and bundle of His are accessed for surgical modification or ablation, a 6 to 7 Fr catheter can be inserted through the femoral vein into the right atrium (diameter ~2 cm at the aortic root) via the inferior vena cava (IVC) (diameter ~2.5 cm) (Fig. 4, blue paths).[117,118]

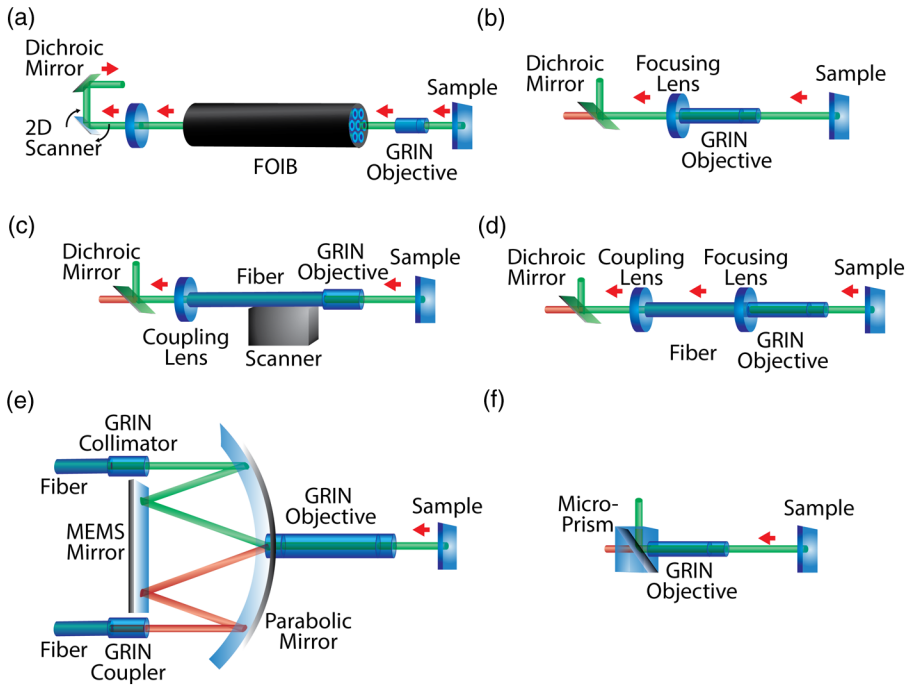

Fig. 3 Microendoscopic systems using gradient index (GRIN) lenses. (a) Scanning FOIB system: Excitation light is scanned across an FOIB and focused on the sample using a GRIN doublet to perform either single-photon confocal imaging[97] or two-photon imaging[98] *in vitro*. (b) Minimally invasive microendoscope using GRIN system: A focusing lens, GRIN doublet, and dichroic mirror can be incorporated in a head-mounted unit to perform *in vivo* single-photon imaging in rat brain[94,99] or *in vivo* two-photon imaging.[94,95,100] (c) Lensed fiber endoscope: Light from a lens fiber is focused onto a sample using a GRIN lens system and scanned across the sample using a raster scanner to perform the single-photon imaging.[101] (d) Light is delivered using a fiber or fiber bundle to a GRIN system which can be mounted on the head of freely moving mice to perform *in vivo* single-photon imaging.[102] (e) Dual-axis confocal microscope: Light is collimated from a single-mode fiber using a GRIN coupler and is focused on to a MEMS system using a parabolic mirror. It is then scanned across a sample using a GRIN-based endoscopic probe to perform *in vitro* and *in vivo* single-photon confocal imaging.[96,103] (f) Portable microendoscope system: A probe consisting of a GRIN doublet fused to a dichroic microprism that can be mounted on to the head of freely moving mice to perform *in vivo* two-photon imaging.[104,105]

Access to the left side of the heart is possible through the femoral artery into the left ventricle via the aorta (diameter ~1.5 cm at arch); however, this approach is typically avoided (because of the higher pressure) or only used for imaging and ablation procedures (Fig. 4, pink paths).[117,118] The brachial cutdown approach can also be used, where the right atrium is accessed through the superior vena cava (SVC) (diameter ~1.5 cm) via the surgically exposed brachial vein (Fig. 4, blue paths).[108,111,118,119] Access to the SA node can also be performed by accessing the coronary arteries using a 5 to 8 Fr catheter through the aorta via the femoral artery (Fig. 4, pink paths).[118] It should be noted that the blood supply to the SA

Table 2 Clinical cardiac imaging modalities using endoscopic access.

Modality	Imaging through blood solution	Advantages	Limitations	Light delivery	Applications
Angioscopy	Balloon occlusion; Flush with optically clear fluid	Direct visualization of surface in color	Photon scattering and absorption by blood	FOIB	Use 6 to 8 Fr (2 to 2.67 mm) catheter to visualize the interior of blood vessels; detect atherosclerotic plaques and thrombi[106,108]
Optical coherence tomography	Balloon occlusion; Flush with optically clear fluid	High resolution (axial: up to 15 μm; lateral: 20 to 25 μm)	Photon scattering and absorption by blood	Single fiber	Use small [~3 Fr (1 mm)] to visualize structures within cardiac tissues, including identification and guidance for stent placement[107,108,110]
Near-IR spectroscopy	Uses near-IR wavelengths which undergo limited scattering	Can image through blood	No anatomical information	FOIB	Detection of lipid core plaque; used with an intravascular ultrasound system inside a 3 Fr (1 mm) catheter in order to provide simultaneous spectral and anatomical information through flowing blood[108,109]

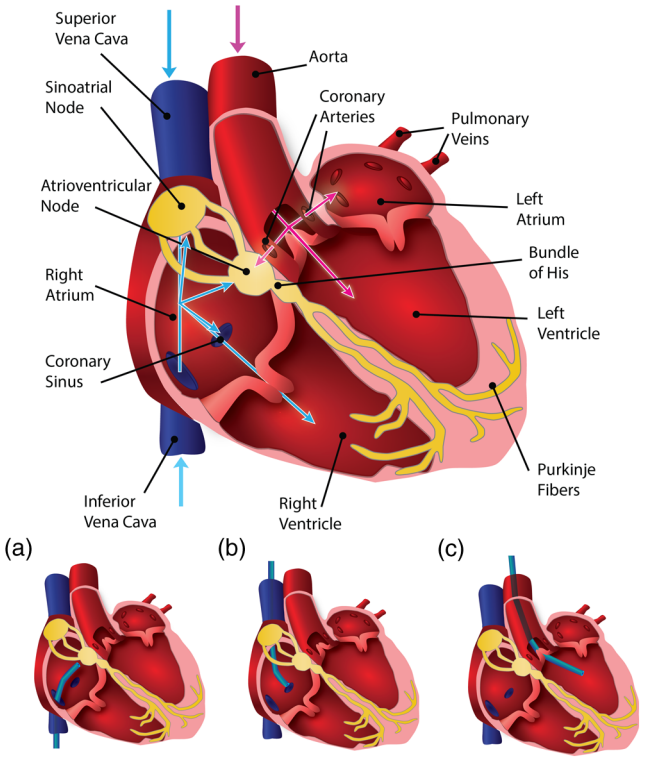

Fig. 4 Schematic of endoscopic paths to access the electrical conduction system of the heart. Blue paths depict the access via the right side of the heart, where a catheter is inserted through the femoral vein to access the right atrium via the inferior vena cava (IVC) or through the brachial vein via the superior vena cava (SVC) (a and b). From the right atrium, the catheter can then access the atrioventricular (AV) node, sinoatrial (SA) node, and bundle of His, or be guided into the coronary sinus (CS) or right ventricle. Pink paths depict the access via the left side of the heart, where a catheter is inserted through the femoral artery in order to access the aorta (c); from there the SA node can be accessed via the coronary arteries or the catheter can be guided into the left ventricle.

node is known to vary, where the right coronary artery (diameter ~2 to 4 mm) provides blood in 50% of patients, the left coronary artery (diameter ~4.5 mm) provides blood in 20% of patients, and in 30% the SA node is supplied by both arteries.[118]

Other important coronary vasculature accessed and used as landmarks for arrhythmia ablation, mapping procedures, and cardiac pacing includes the coronary sinus (CS, diameter 7.5 to 11.5 mm), which can be accessed via the right atrium (Fig. 4, blue paths).[120,121] In addition, tributaries to the CS are the great cardiac vein (diameter 8.3 ± 1.7 mm), middle cardiac vein (diameter ~3 to 5.5 mm), left marginal vein (diameter ~1 to 3 mm), the vein of Marshall (diameter ~1 mm), the anterior interventricular vein (diameter 2 to 3 mm), and the posterior cardiac vein (diameter 1.5 to 3.5 mm) and can be used for pacing the left ventricle.[121] To navigate through the heart *in vivo*, we intend to design a system to be easily integrated into current cardiac catheterization techniques.

6 Design of a Microendoscopic System for All-Optical Cardiac Interrogation

Optical actuation and recording of the heart *in vivo* are limited by both its ability to collect and detect light because of the inherent size constraints of *in vivo* microendoscopic imaging and

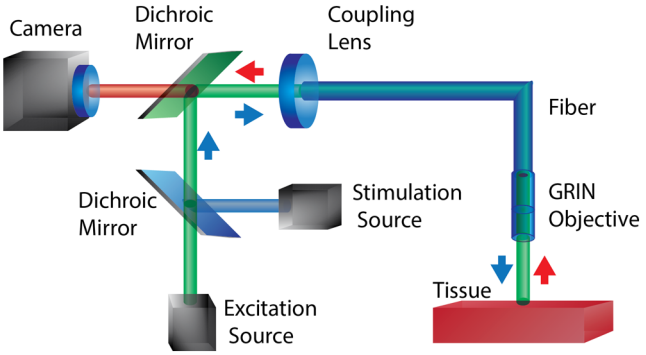

Fig. 5 Optical path diagram of proposed fiber-optic based microendoscopic device for cardiac optogenetics. Excitation light for the fluorescent dye is combined with stimulation light using a dichroic mirror, and both beams are coupled into an optical fiber using a fiber coupler. Light from the fiber is focused on to the sample using an endoscopic probe. The fluorescent signal is then coupled back into the fiber using the same probe and sent to the detector using a dichroic mirror.

the low-signal strengths of fluorescent probes. Both fast optics (i.e., optics with high NA and thus ability to capture low-light fast events) and high-speed detectors with large quantum efficiencies are needed in order to account for low-light intensities due to photon scattering and absorption. In addition, use of a single probe and single actuator requires the accommodation of three wavelengths: the excitation and emission wavelengths of the fluorescent indicator and the stimulation wavelength for the genetically encoded actuator.

The proposed solution for an *in vivo* fiber-based cardiac optogenetics system utilizes techniques already used for fiber-based cardiac imaging and *in vivo* neural optogenetics, with the addition of technology used in microendoscopy to provide the high light collection ability. The generalized schematic of the proposed system can be seen in Fig. 5. The system requires two light sources: one for excitation of the fluorescent indicator and the other to act as a stimulation source for the light-sensitive ion channel. The two beams will be coupled into an optical fiber and focused onto the sample using a microendoscopic-like probe. Emitted fluorescent light from the sample will then be coupled back into the fiber and separated from the excitation and stimulation light using a second beam splitter and will finally be imaged on to a detector. In this section, we will outline the physical constraints for such a system and how can it be constructed by borrowing ideas from cardiac imaging, microendoscopy, and optogenetics.

6.1 *Challenges*

6.1.1 *Photon scattering and absorption*

Photon penetration depth is determined by both scattering and absorption within media. The intensity of light of wavelength λ at a depth z within the tissue is defined as

$$I(z) = I_0 e^{-[\mu_a(\lambda)+\mu_s(\lambda)]z}, \quad (1)$$

where I_0 is the initial light intensity, and $\mu_a(\lambda)$ and $\mu_s(\lambda)$ are the wavelength-dependent absorption and scattering coefficients, respectively. Very recently, valuable photon absorption and scattering data for visible wavelengths were reported for the rat heart, where the $\mu_a(\lambda)$ peaks at 450 and 550 nm and

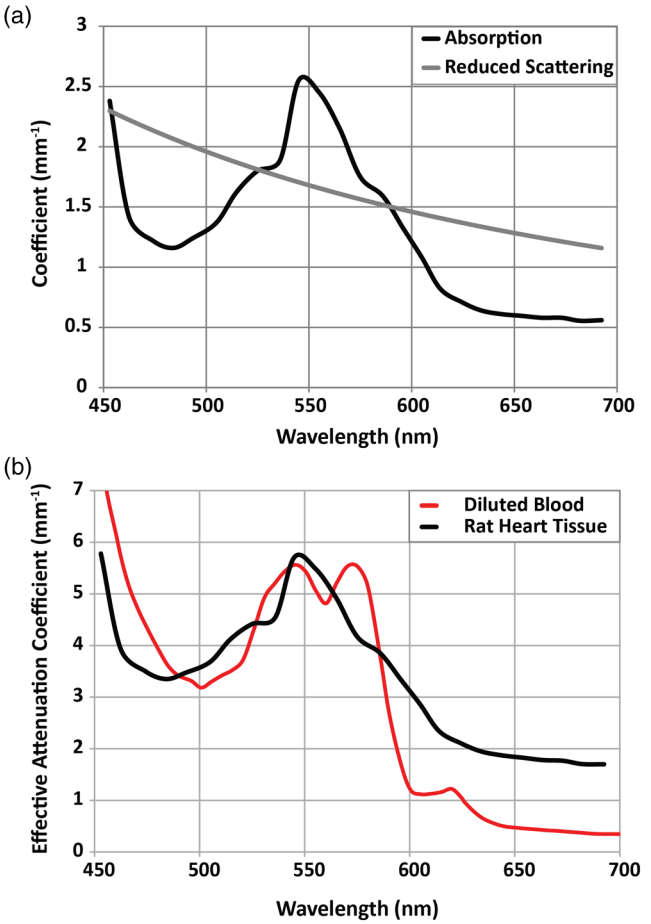

Fig. 6 Scattering and absorption data for rat heart tissue. (a) Absorption and reduced scattering coefficients for visible wavelengths in the rat heart (adapted from Ref. 122); (b) effective attenuation coefficients for visible wavelengths in rat heart tissue (adapted from Ref. 122) and diluted blood at 100% O_2 saturation (adapted from Ref. 123).

$\mu_s(\lambda)$ follows Rayleigh scattering and decreases monotonically with the increase in wavelength.[122] This information has been adapted in Fig. 6(a), which shows the absorption, scattering, and attenuation coefficients in the visible spectrum for heart tissue. Figure 6(b) compares the effective attenuation coefficients for diluted blood and rat heart tissue; unsurprisingly, the absorption peak for heart tissue is close to that of hemoglobin. These data are informative for the design of optogenetic probes (for actuation and imaging) with suitable spectral characteristics for *in vivo* use.

Because of the large attenuation of visible wavelengths within the cardiac tissue, imaging at the endocardial surface and subsurface and optical access to the conduction system of the heart cannot be performed from outside the heart. Access to the epicardial surface is impractical for routine clinical procedures, as it requires invasive, open-chest surgery to expose the heart. Thus, endoscopic approaches have become standard for clinical cardiac imaging procedures.

6.1.2 *Vasculature and size constraints for endoscopy*

To optically actuate and record from the endocardial surface, the imaging system must be small enough to be used in cardiac catheterization procedures. As discussed previously, the conduction system is most easily accessed from the right atrium, where the catheter enters through either the SVC or IVC. Although the data above are for humans, allometric (power-law) scaling provides a convenient way to relate cardiovascular parameters in various animals. In mammals, the major blood vessels and their branches (but not capillaries) obey allometric laws. The relationship between some physiological dimension y and body mass M in kg is given by

$$y = aM^b, \tag{2}$$

where a and b are the scaling factors.[124,125] Sizes of vasculature relevant for cardiac catheterization procedures have been calculated using scaling parameters empirically derived in Holt et al.[124] and summarized in Table 3. For endoscopic use in rats, for example, the optical system will need to be less than ~2.5 mm in diameter to access the right heart. Constraining the system to 1-mm diameter would allow for easier navigation and is within the constraints of available optical components, which will be discussed in the next section. These sizes are within the capabilities of current microendoscopy techniques. Further analysis of the curvature is needed depending on the chosen access path in order to assess potential light losses and feasibility.

6.1.3 *Motion artifacts*

Mechanical contractions of the heart pose a particular challenge to *in vivo* cardiac imaging by creating motion artifacts in the optically measured signal. In neuroscience, optical systems can be physically mounted to the subject's skull, allowing the subject to freely move while keeping the detection system relatively stationary with respect to brain structures. However, no such rigid structure surrounds the heart, and the heart itself would still be constantly moving. For *in vitro* optical mapping, motion uncouplers, such as 2,3-butanedione monoxime[9,13,14] and Blebbistatin,[46–48] are used to reduce motion artifacts; however, their effect on the electrical properties of the tissue makes them unsuitable for use *in vivo*. Ratiometric techniques and dual-wavelength subtraction provide a drug-free alternative to filtering motion artifacts, with the latter of the two having already been used for fiber-optic cardiac imaging.[15,45,49] However, both these options require the system to accommodate an additional (fourth) wavelength.

A practical approach involves looking at clinical techniques used to avoid complications due to heart wall motion for chronically implanted pacing leads as inspiration for an endoscopic imaging system. For example, long-term treatment of bradycardia requires flexible pacing electrodes at the endocardial surface within the right atrium. To prevent the dislodgment, the electrode is physically fixed to the endocardial surface via passive or active fixation methods.[126] Passive fixation is the most commonly used, where flexible tines or fins entrap the lead within the trabeculae; however, these leads are susceptible to fibrotic encapsulation, making them almost impossible to remove.[126] Active fixation provides a more suitable alternative for endoscopic imaging, where a corkscrew tip is used to directly screw the lead into the endocardial wall.[126] This provides much more flexibility in lead placement within the right atrium and ventricle and allows for the device to be removed if necessary.[126] Additional stabilization techniques can involve the combination of the microendoscopic guide with a deployable stent-like structure to keep in place.

Table 3 Allometric (power-law) scaling of vasculature[124] and calculated dimensions for relevant vasculature (in centimeter) for the mouse, rat, canine, goat, and human. AA—ascending aorta; CA—coronary artery; BA—brachiocephalic artery; SVC—superior vena cava; IVC—inferior vena cava.

Variables (cm)	a	b	Mouse (0.025 kg)	Rat (0.225 kg)	Canine (25 kg)	Goat (50 kg)	Human (70 kg)
ØAA	0.41	0.36	0.11	0.24	1.31	1.68	1.89
Ø Aorta at one-fourth length	0.34	0.36	0.09	0.20	1.08	1.39	1.57
Ø Left CA	0.1	0.36	0.03	0.06	0.32	0.41	0.46
Ø BA	0.24	0.37	0.06	0.14	0.79	1.02	1.16
Ø SVC at heart	0.46	0.41	0.10	0.25	1.72	2.29	2.63
Ø IVC at heart	0.48	0.41	0.11	0.26	1.80	2.39	2.74
Ø IVC at one-fourth length	0.83	0.26	0.32	0.56	1.92	2.30	2.50
Length aorta; valves—BA	1	0.28	0.36	0.66	2.46	2.99	3.29

6.1.4 *Combined optical recording and actuation: probes and spectral considerations*

Cardiac optical mapping achieves superior spatial resolution compared with electrodes by employing fluorescent probes. Probe selection is dependent on both response speed and signal strength to perform the high-spatiotemporal resolution imaging on the millisecond timescale. The two key classes of fast response indicators are voltage (potentiometric) and calcium probes; examples of these indicators can be seen in Table 1. For *in vitro* voltage sensing, the styryl dyes di-4-ANEPPS, di-8-ANEPPS, and RH-237 undergoing spectral shifts that vary linearly with voltage changes have been used extensively in optical mapping[5–7,30,31,35,38,40,127,128] and other cardiac imaging systems.[12–15,44,46–48] However, these potentiometric dyes are inherently inefficient. For example, di-4-ANEPPS has a quantum efficiency estimated to be on the order of 0.3[129,130] and is excited at irradiances as low as 0.1 up to 5 mW/mm^2 before light-induced tissue heating occurs[128] resulting in, at best, a 10% relative change in fluorescence per 100 mV.[5] More recently, new near-infrared dyes, such as di-4-ANBDQPQ and di-4-ANBDQBS, have been used in blood-perfused hearts as their absorption peak is >70 nm higher than that of hemoglobin.[5,131]

The cycling of intracellular calcium is also of interest for understanding cardiac electrophysiology and is an essential part of excitation-contraction coupling within cardiomyocytes.[5,6] Unlike potentiometric dyes, commonly used calcium dyes, such as Fluo-4, Fluo-3, and Fura-2, have much stronger optical signals, thus imaging is typically not limited by the efficiency of these dyes; however, these probes do not capture the action potential itself, and certain probes, such as Fluo-4 and Fura-2, are known to prolong calcium transients.[5–7] Fluo-3, Fluo-4, Rhod-2, and Rhod-4 are commonly used dyes excited by blue-green wavelengths that can be employed in conjunction with voltage-sensitive dyes RH-237 and the red-shifted Di-4-ANBDQPQ. The UV-excited Fura-2 has also been used, including in conjunction with Di-4-ANBDQPQ.[32]

For *in vivo* use, genetically encoded indicators with excitation and absorption spectra suitable for imaging through blood will be necessary. For *in vivo* calcium imaging, genetically encoded GCaMP variants, which use GFP as the fluorescent reporter, are commonly used. The most recent variant, GCaMP6, shows great promise for speed and high SNR.[132] The creation of genetically encoded, fast-voltage sensors has been challenging, yet some successful probes have recently been generated such as voltage-sensitive fluorescent proteins (VSFPs). The VSFP variant VSFP3 (based on a phosphatase voltage-sensing domain) includes a promising indicator based on mKate as the reporter, though speed remains an issue.[132] Recently, genetically encoded opsins, such as mutants of Arch, have been adapted as voltage sensors.[133] The Arch-derived sensor Arch(D95H) has been shown to have the fluorescence response variations in both amplitude and time course due to voltage change.[134,135] In addition, the Arch variants Arch-EEN and Arch-EEQ have also been demonstrated as voltage sensors with faster kinetics and larger signal intensities compared with Arch(D95H).[136]

The key challenge to combine all actuation and sensing is cleanly separating wavelengths for optogenetic stimulation and fluorescent excitation and emission with sufficient resolution. Ideally, the actuators should be chosen such that their absorption spectrum lies either above or below the excitation and emission spectra of the probe. Spectral separation can be further augmented by careful selection of excitation and emission filters and dichroic mirrors. In cases where the absorption spectrum of the actuator does not lie below both spectra of the sensor, a notch or multiedge rather than a long-pass dichroic mirror can be used to separate the emitted fluorescence from the combined light sources, without requiring major modifications to the optical system. Other spectral issues, not as easily addressed by simple filtering, may arise. For example, as seen in Table 1, ChR2 and Rhod-4 are compatible for use in the same optical system and have been used in combined actuation and sensing in cardiac tissue.[85,137] However, ChR2 has an intermediate deactivating green state at 520 nm after activation with 480 nm,[138] and, therefore, this combination may not be ideal. Some actuators are fundamentally incompatible with commonly used sensors, where their absorption spectra either overlap or lie in between the excitation and emission spectra of the sensor. For example, the spectra of hyperpolarizing opsins, such as NpHR, lie between the excitation and emission spectra of commonly used sensors such as Di-8 and Rhod-4. Thus, shorter wavelength sensors, such as Fura-2, have been used to monitor

the modulation of neurons in neonatal mouse cortical slices by both hyperpolarizing NpHR and depolarizing ChR2.[54] From the more relevant for *in vivo* use genetically encoded sensors, the calcium sensor G-CaMP has been used to map functional connections in ChR2-expressing neurons of *Caenorhabditis elegans*, as a demonstration of an all-optical approach.[139] Very recent work also shows the possibility to use genetically encoded voltage sensors *in vivo*.

In addition to spectral overlap of optical actuators and sensors, spectral overlap of the probes and the absorption peaks of both tissue and blood must also be considered to optimize the light delivery and detection. As can be seen in Fig. 6(b), although scattering increases for shorter wavelengths, the effective attenuation coefficient of light in tissue mimics that of diluted blood across visible wavelengths, peaking at 550 nm. Thus, for optimal penetration depth, red-shifted sensors must be used. Two-photon illumination, which allows for red-shifted light to be used for excitation, can also be used. However, this method requires higher irradiances, which can lead to tissue heating.[77]

6.2 *Imaging System*

6.2.1 *Optical fibers*

Optical fibers are commonly used in both microendoscopy and optogenetics in neuroscience to remotely deliver and collect light deep within the tissue. Fiber selection is dependent on the choice of wavelengths, the diameter of the optical system, and the choice of collection optics; the NA of the fiber must be matched to that of the optics in order to maximize the collection efficiency of the system. Step-index fibers are the most commonly used, where light is guided using total internal reflection through a core, surrounded by a lower index of refraction cladding. The diameter of the core determines the wavelength ranges that can be efficiently coupled, the number of spatial modes that can be transmitted, and the NA. For visible wavelengths, step-index single-mode fibers have core diameters between 3 and 6 μm and NAs up to 0.13 NA, while multimode fibers have larger core diameters (10 μm to 1 mm) giving them larger NAs (0.1 to 0.48 NA). Step-index fibers, however, are only able to transmit the intensity information and are subjected to intermodal dispersion due to different modes propagating at different velocities through the core.

In order to accommodate three wavelengths (excitation, stimulation, and emission), maximize the light collection efficiency and perform the multipoint imaging, a bundle of multimode optical fibers would be the ideal choice for an all-optical actuation system. FOIBs are commonly used in multipoint imaging microendoscopic systems in neuroscience including for *in vivo* optical mapping. The resolution of the FOIB is limited by both the core-to-core spacing of the individual bundles as well as the NA of the fiber bundle. The IGN-08/30 Sumitomo FOIB has been used in multiple microendoscopic systems[97,98,102,140] including for Ca^{2+} calcium imaging in freely behaving mice.[102] The 0.35-NA jacketed bundle has an outer diameter of <1 mm and consists of 30,000 individual fibers with a core-to-core spacing of ~4 μm, core diameter of ~2.4 μm, and bending radius of 40 mm,[102] making it a potentially suitable option for *in vivo* cardiac approaches. The bending radius may be too large for rodent subjects, but standard optical fibers have bending radii ranging from 10 to 40 mm.

6.2.2 *Optics*

Due to photon scattering and absorption and low-quantum efficiencies of currently available fluorescent reporters, the optical system must collect as much light as possible. The effective NA of the microendoscopic objective dictates both the spatial resolution and the light-gathering ability—the latter directly affecting the limits of the temporal resolution of the optical system. Although traditional microscope objectives have been used for fiber-based systems,[88–92,140–142] even small diameter, custom-made objectives have been too bulky for most *in vivo* applications and only provide a modest light-gathering ability (<0.35 NA).

The collection efficiency of an optical system is dependent on the solid angle Ω subtended by the collection optics and is related to the NA of the system by

$$\frac{\Omega}{4\pi} = \frac{1}{2}\left(1 - \sqrt{1 - \mathrm{NA}^2}\right). \tag{3}$$

Optical fibers alone typically have small collection efficiencies; for example, multimode optical fibers with NAs between 0.1 and 0.48 only have collection efficiencies of 0.0025 to 0.061. However, using fiber-coupling or collimation systems designed to have NAs between 0.5 and 0.8, collection efficiencies between 0.07 and 0.2 can be achieved.

As discussed above, small diameter microendoscopic imaging has benefited from the recent development of GRIN optics, which range from 0.35 to 1 mm in diameter and have NAs as high as 0.65. GRIN lenses are used as singlet, doublet, or triplet systems and can be combined with plano-convex lenses.[93] Typically, doublet systems are used for higher-NA systems, whereas triplet systems employ an extra relay lens to lengthen the objective for deeper imaging. GRIN lenses used in conjunction with plano-convex microlenses are best suited for high-resolution systems, where the GRIN objectives can be designed to compensate for aberrations from the plano-convex lens.[93]

Selection of a GRIN objective is determined by the FOV of the optical system, which is usually limited by the diameter of the optical system. Wider GRIN objectives have larger FOVs and NAs, but this is commonly accompanied by longer WDs. For the single-photon microendoscopic systems used in neuroscience, the WD is limited to approximately 0.1 mm from the endoscopy tip, as at longer distances photon scattering and absorption greatly decrease the SNR.[93] In GRIN doublet objectives, the relay lens is selected based on the NA of the collection optics; the NA must be equal to or smaller than that of the optical fibers or FOIBs to ensure an efficient coupling. GRIN doublet systems have been used with FOIBs for microendoscopic imaging *in vivo*[98,102] including performing video-rate Ca^{2+} recordings using an EMCCD camera in freely moving mice.[102] However, a large portion of the imaging system was mounted outside the animal's skull, allowing larger diameter optics to be employed: a 2 mm diameter coupling lens, a 2 mm diameter focusing lens, and a 1 mm objective with 0.47 NA.[102] A similar scanning microendoscope system consisting of 1 mm diameter optics, a relay lens of 0.2 NA and an objective lens of 0.5 NA, to couple into a 0.35 NA FOIB will be a more suitable model for cardiac use.[98]

6.2.3 *Illumination*

High quality light sources for both excitation of fluorescent dyes and optical actuation are necessary to produce an effective cardiac optogenetic imaging and actuation system. When selecting a light source, the key features that must be considered include the source's spectrum, power, stability and controllability (maximum frequency the source can be pulsed for optical actuation). For optical actuation of cardiac tissue, the source must be capable of variable intensity control that can be pulsed or switched at speeds relevant for cardiac pacing, typically 0.1 to 5 mW/mm^2 irradiances at the site of actuation and 0.5–12 Hz pacing frequencies. The required optical power for imaging must be sufficient to excite the fluorescent probe but without causing tissue heating. For example, di-4-ANEPPS and di-4-ANBDQBS (excited by 535 nm and 660 nm, respectively) show little difference in percent of fluorescence change during an action potential for irradiances varied from 0.1 to 5 mW/mm^2; however, at higher irradiances, tissue heating can occur thereby altering the measured action potentials.[128] Other practical considerations include the power consumption of the light source, whether or not cooling units are needed, the size of the device, and how easily the light source can be coupled into the system.

Advances in solid-state technology have led to the availability of cost-effective LED-based light sources that are a more practical alternative to traditionally used broad-spectrum arc lamps, as they can be pulsed using frequencies well over 1 kHz using digital pulses (e.g., TTL pulses, which act as a binary on/off switch) or analog modulation. Although they can be purchased as fiber-coupled units at specific wavelengths, they are incoherent sources (typically having bandwidths of 10 nm) causing considerable intensity loss when coupled into optical fibers. However, new LED technologies show promise for miniaturized systems that do not require the light sources to be fiber coupled. For *in vivo* use, new semiconductor fabrication techniques have allowed for the fabrication of μLEDs ($1000 \times 600 \times 200$ μm^3) for miniaturized probes that can be directly inserted into tissue.[73] Also, recently flexible, stretchable μLED arrays have been manufactured and used in balloon-based catheters; these sheets could also be placed on the heart in order to provide on-site illumination.[143]

For applications requiring coherent, high-intensity light, lasers are preferred, as they can be tightly focused and efficiently coupled into optical fibers. They are more expensive than LED-based options and not all laser types can be as reliably pulsed using digital or analog modulation. Of particular interest are solid state lasers, including direct diode lasers, diode pumped solid state (DPSS) lasers, and optically pumped semiconductor lasers, available in a range of wavelengths with narrow bandwidths (<1 nm). Certain laser types, such as DPSS lasers, are known to have unpredictable power stabilities when modulated with TTL pulses, complicating optogenetic stimulation, but they are still attractive for fluorescence excitation which requires continuous illumination.

6.2.4 *Detectors*

Small diameter optical systems have limited collection efficiencies, thus special consideration must be made when choosing a detector, including the detector's quantum efficiency at the wavelengths of the fluorescent reporter being used, active area compared with the system's aperture size, and SNR at the needed temporal resolution. For optical mapping, acquisition rates must be at least 200 Hz,[6] and as red-shifted fluorescent probes are more desirable due to less scattering and absorption at longer wavelengths, detectors with quantum efficiency peaks in the red are preferred.

Single-point detectors are commonly used in both single-point imaging as well as multipoint imaging employing scanning systems or detector arrays. PMTs are among the most commonly used detectors in fluorescence detection and microendoscopy, as they have high gain (typically on the order of 10^6) and relatively low noise. Although they can be purchased with relatively large detector areas, they require high voltages to stably operate and their quantum efficiency is poor in the near-IR range (<20%). Solid state detectors, such as avalanche photodiodes (APDs) have higher quantum efficiencies in the longer wavelengths (50 to 90%). APDs perform like a solid-state version of a PMT, where gains on the order of 1000 can be achieved; however, they have much smaller active areas compared with PMTs. Single-photon counting modules are a specific subset of APDs that can be used for detecting extremely small signals, including single-photon detection. Although these detectors are able to measure low-intensity signals with high-quantum efficiency in the near-IR (>60%), they have very small active diameters, typically less than 200 μm.

High-resolution CCD cameras and EMCCD cameras have been popular for use in optical mapping[5–7,30–34,37–40,127,128,144] and microendoscopy due to their high-spatiotemporal resolution. EMCCD cameras take advantage of avalanche processes to perform the on-chip electron multiplication to enhance SNRs, have higher frame rates, and improved quantum efficiency.[5] Current EMCCD models, such as the Andor iXon Ultra 897, have 512×512 pixels and can achieve full-frame rates of 56 frames per second; this rate be increased to above 100 frames per second by employing crop modes. EMCCD cameras have been used in optical mapping systems and in microendoscopic systems, including for recording video rate Ca^{2+} imaging in freely moving mice using a FOIB and a GRIN objectives.[102] In addition to using fiber-based systems, microendoscope probes have also incorporated miniaturized cameras mounted directly on to the subject. Recently, miniaturized CMOS cameras have been incorporated into miniature, head-mounted microendoscopes for imaging calcium transients in behaving mice.[99] Since spatial mapping is of interest in cardiac applications, EMCCD and newer CMOS detectors with suitable characteristics are most desirable.

7 Conclusions

Furthering our understanding of cardiac electrophysiology, as related to pacemaking, arrhythmogenesis, and cardioversion, requires precise, spatially localized and cell-specific actuation and measurement of electrical activity *in vivo*. Optical mapping currently provides high-spatiotemporal resolution visualization of the propagation of electrical signals through cardiac syncytium *in vitro* or *in situ*. When combined with cardiac optogenetics, high-spatiotemporal resolution all-optical interrogation can be performed. Cell-specific actuation and mapping of internal structures of interest, e.g., the conduction system, are currently impossible as optical recordings are limited to the epicardial surface and subsurface due to photon scattering and absorption.

Although optogenetics studies in neuroscience in intact mammals have become standard practice, no such experiments have been performed in the heart due to the lack of available technologies. To perform all-optical electrophysiological actuation

and sensing in the heart *in vivo*, an imaging system is necessary that can navigate to the heart via catheterization procedures while still maintaining sufficient light-collection ability. The design of such a device must address: (1) spectral challenges due to using multiple fluorescent probes; (2) photon scattering and absorption of cardiac tissue; (3) navigation through small-diameter vasculature to access the endocardial surface; and (4) optical artifacts due to the motion of the heart wall. By combining solutions from microendoscopic approaches and current clinical cardiac catheterization procedures, such a system can be realized. This would provide a means to test and validate newly developed genetically encoded actuators and sensors, allowing for the expansion of cardiac optogenetics to *in vivo* applications and a better understanding of cardiac electrophysiology as a whole.

Acknowledgments

Our work on cardiac optogenetics is supported by NIH-NHLBI Grant R01HL111649 (EE). We acknowledge helpful discussions with Christina M. Ambrosi, PhD, and other members of the Entcheva lab.

References

1. C. M. Ambrosi et al., "Termination of sustained atrial flutter and fibrillation using low-voltage multiple-shock therapy," *Heart Rhythm* **8**(1), 101–108 (2011).
2. A. H. Janardhan et al., "Multistage electrotherapy delivered through chronically-implanted leads terminates atrial fibrillation with lower energy than a single biphasic shock," *J. Am. Coll. Cardiol.* **63**(1), 40–48 (2014).
3. F. G. Akar and R. J. Hajjar, "Gene therapies for arrhythmias in heart failure," *Pflugers Arch.* **466**(6), 1211–1217 (2014).
4. L. Tilemann et al., "Gene therapy for heart failure," *Circ. Res.* **110**(5), 777–793 (2012).
5. T. J. Herron, P. Lee, and J. Jalife, "Optical imaging of voltage and calcium in cardiac cells & tissues," *Circ. Res.* **110**(4), 609–623 (2012).
6. E. Entcheva and H. Bien, "Macroscopic optical mapping of excitation in cardiac cell networks with ultra-high spatiotemporal resolution," *Prog. Biophys. Mol. Biol.* **92**(2), 232–257 (2006).
7. I. R. Efimov, V. P. Nikolski, and G. Salama, "Optical imaging of the heart," *Circ. Res.* **95**(1), 21–33 (2004).
8. G. Nagel et al., "Channelrhodopsin-1: a light-gated proton channel in green algae," *Science* **296**(5577), 2395–2398 (2002).
9. G. Nagel et al., "Channelrhodopsin-2, a directly light-gated cation-selective membrane channel," *Proc. Natl. Acad. Sci. U. S. A.* **100**(24), 13940–13945 (2003).
10. K. Deisseroth et al., "Next-generation optical technologies for illuminating genetically targeted brain circuits," *J. Neurosci.* **26**(41), 10380–10386 (2006).
11. E. Entcheva, "Cardiac optogenetics," *Am. J. Physiol. Heart Circ. Physiol.* **304**(9), H1179–H1191 (2013).
12. V. Krauthamer et al., "Action potential-induced fluorescence changes resolved with an optical fiber carrying excitation light," *J. Fluoresc.* **1**(4), 207–213 (1991).
13. D. A. Hooks et al., "Intramural multisite recording of transmembrane potential in the heart," *Biophys. J.* **81**(5), 2671–2680 (2001).
14. J. L. Byars et al., "Development of an optrode for intramural multisite optical recordings of Vm in the heart," *J. Cardiovasc. Electrophysiol.* **14**(11), 1196–1202 (2003).
15. N. H. Brown et al., "A fiber-based ratiometric optical cardiac mapping channel using a diffraction grating and split detector," *Biophys. J.* **93**(1), 254–263 (2007).
16. G. Gao et al., "Transendocardial delivery of AAV6 results in highly efficient and global cardiac gene transfer in rhesus macaques," *Hum. Gene Ther.* **22**(8), 979–984 (2011).
17. J. J. Chong et al., "Human embryonic-stem-cell-derived cardiomyocytes regenerate non-human primate hearts," *Nature* **510**(7504), 273–277 (2014).
18. G. Salama and M. Morad, "Merocyanine 540 as an optical probe of transmembrane electrical activity in the heart," *Science* **191**(4226), 485–487 (1976).
19. M. Morad and G. Salama, "Optical probes of membrane potential in heart muscle," *J. Physiol.* **292**, 267–295 (1979).
20. L. Cohen and B. Salzberg, "Optical measurement of membrane potential," in *Reviews of Physiology, Biochemistry and Pharmacology*, Vol. 83, pp. 35–88, Springer, Berlin, Heidelberg (1978).
21. A. Grinvald, "Real-time optical mapping of neuronal activity: from single growth cones to the intact mammalian brain," *Annu. Rev. Neurosci.* **8**, 263–305 (1985).
22. D. S. Rosenbaum et al., "Repolarization inhomogeneities in ventricular myocardium change dynamically with abrupt cycle length shortening," *Circulation* **84**(3), 1333–1345 (1991).
23. I. R. Efimov et al., "Optical mapping of repolarization and refractoriness from intact hearts," *Circulation* **90**(3), 1469–1480 (1994).
24. B. R. Choi and G. Salama, "Optical mapping of atrioventricular node reveals a conduction barrier between atrial and nodal cells," *Am. J. Physiol. Heart Circ. Physiol.* **274**(3), H829–H845 (1998).
25. C. Cabo et al., "Wave-front curvature as a cause of slow conduction and block in isolated cardiac muscle," *Circ. Res.* **75**(6), 1014–1028 (1994).
26. W. T. Baxter et al., "Technical features of a CCD video camera system to record cardiac fluorescence data," *Ann. Biomed. Eng.* **25**(4), 713–725 (1997).
27. C. J. Hyatt et al., "Synthesis of voltage-sensitive fluorescence signals from three-dimensional myocardial activation patterns," *Biophys. J.* **85**(4), 2673–2683 (2003).
28. F. H. Samie et al., "Rectification of the background potassium current: a determinant of rotor dynamics in ventricular fibrillation," *Circ. Res.* **89**(12), 1216–1223 (2001).
29. B. R. Choi et al., "Life span of ventricular fibrillation frequencies," *Circ. Res.* **91**(4), 339–345 (2002).
30. A. D. Bachtel et al., "A novel approach to dual excitation ratiometric optical mapping of cardiac action potentials with di-4-ANEPPS using pulsed LED excitation," *IEEE Trans. Biomed. Eng.* **58**(7), 2120–2126 (2011).
31. E. B. Bourgeois et al., "Simultaneous optical mapping of transmembrane potential and wall motion in isolated, perfused whole hearts," *J. Biomed. Opt.* **16**(9), 096020 (2011).
32. P. Lee et al., "Single-sensor system for spatially resolved, continuous, and multiparametric optical mapping of cardiac tissue," *Heart Rhythm* **8**(9), 1482–1491 (2011).
33. P. Lee et al., "Simultaneous measurement and modulation of multiple physiological parameters in the isolated heart using optical techniques," *Pflugers Arch.* **464**(4), 403–414 (2012).
34. P. Lee et al., "In situ optical mapping of voltage and calcium in the heart," *PLoS One* **7**(8), e42562 (2012).
35. L. Tang et al., "Intracellular calcium dynamics, shortened action potential duration, and late-phase 3 early afterdepolarization in Langendorff-perfused rabbit ventricles," *J. Cardiovasc. Electrophysiol.* **23**(12), 1364–1371 (2012).
36. G. Bub et al., "Temporal pixel multiplexing for simultaneous high-speed, high-resolution imaging," *Nat. Methods* **7**(3), 209–211 (2010).
37. B. J. Caldwell et al., "Probing field-induced tissue polarization using transillumination fluorescent imaging," *Biophys. J.* **99**(7), 2058–2066 (2010).
38. W. T. Baxter et al., "Visualizing excitation waves inside cardiac muscle using transillumination," *Biophys. J.* **80**(1), 516–530 (2001).
39. B. G. Mitrea, B. J. Caldwell, and A. M. Pertsov, "Imaging electrical excitation inside the myocardial wall," *Biomed. Opt. Express* **2**(3), 620–633 (2011).
40. R. D. Walton et al., "Extracting surface activation time from the optically recorded action potential in three-dimensional myocardium," *Biophys. J.* **102**(1), 30–38 (2012).
41. P. M. Boyle et al., "A comprehensive multiscale framework for simulating optogenetics in the heart," *Nat. Commun.* **4**, 2370 (2013).
42. E. M. Hillman et al., "Depth-resolved optical imaging of transmural electrical propagation in perfused heart," *Opt. Express* **15**(26), 17827–17841 (2007).
43. V. Krauthamer, C. C. Davis, and E. T. Gan, "Two-point electrical-fluorescence recording from heart with optical fibers," *IEEE Trans. Biomed. Eng.* **41**(12), 1191–1194 (1994).

44. M. Neunlist, S. Zou, and L. Tung, "Design and use of an "optrode" for optical recordings of cardiac action potentials," *Pflugers Arch.* **420**(5), 611–617 (1992).
45. D. C. Tai et al., "Correction of motion artifact in transmembrane voltage-sensitive fluorescent dye emission in hearts," *Am. J. Physiol. Heart Circ. Physiol.* **287**(3), H985–H993 (2004).
46. W. Kong et al., "Optical measurements of intramural action potentials in isolated porcine hearts using optrodes," *Heart Rhythm* **4**(11), 1430–1436 (2007).
47. W. Kong, R. E. Ideker, and V. G. Fast, "Intramural optical mapping of V(m) and Ca(i)2+ during long-duration ventricular fibrillation in canine hearts," *Am. J. Physiol. Heart Circ. Physiol.* **302**(6), H1294–H1305 (2012).
48. W. Kong, A. E. Pollard, and V. G. Fast, "A new optrode design for intramural optical recordings," *IEEE Trans. Biomed. Eng.* **58**(11), 3130–3134 (2011).
49. B. J. Caldwell et al., "Intramural measurement of transmembrane potential in the isolated pig heart: validation of a novel technique," *J. Cardiovasc. Electrophysiol.* **16**(9), 1001–1010 (2005).
50. G. J. Kong et al., "Lensed photonic crystal fiber obtained by use of an arc discharge," *Opt. Lett.* **31**(7), 894–896 (2006).
51. E. S. Boyden et al., "Millisecond-timescale, genetically targeted optical control of neural activity," *Nat. Neurosci.* **8**(9), 1263–1268 (2005).
52. G. Nagel et al., "Light activation of channelrhodopsin-2 in excitable cells of Caenorhabditis elegans triggers rapid behavioral responses," *Curr. Biol.* **15**(24), 2279–2284 (2005).
53. H. Wang et al., "High-speed mapping of synaptic connectivity using photostimulation in Channelrhodopsin-2 transgenic mice," *Proc. Natl. Acad. Sci. U. S. A.* **104**(19), 8143–8148 (2007).
54. F. Zhang et al., "Multimodal fast optical interrogation of neural circuitry," *Nature* **446**(7136), 633–639 (2007).
55. J. Wang et al., "A neurophotonic device for stimulation and recording of neural microcircuits," in *2010 Annual Int. Conf. of the IEEE Engineering in Medicine and Biology*, Buenos Aires, IEEE (2010).
56. B. Y. Chow et al., "High-performance genetically targetable optical neural silencing by light-driven proton pumps," *Nature* **463**(7277), 98–102 (2010).
57. N. C. Klapoetke et al., "Independent optical excitation of distinct neural populations," *Nat. Methods* **11**(3), 338–346 (2014).
58. A. M. Aravanis et al., "An optical neural interface: in vivo control of rodent motor cortex with integrated fiberoptic and optogenetic technology," *J. Neural Eng.* **4**(3), S143–S156 (2007).
59. Y. Hayashi et al., "Spatio-temporal control of neural activity in vivo using fluorescence microendoscopy," *Eur. J. Neurosci.* **36**(6), 2722–2732 (2012).
60. C. T. Wentz et al., "A wirelessly powered and controlled device for optical neural control of freely-behaving animals," *J. Neural Eng.* **8**(4), 046021 (2011).
61. A. M. Leifer et al., "Optogenetic manipulation of neural activity in freely moving Caenorhabditis elegans," *Nat. Methods* **8**(2), 147–152 (2011).
62. A. R. Adamantidis et al., "Neural substrates of awakening probed with optogenetic control of hypocretin neurons," *Nature* **450**(7168), 420–424 (2007).
63. X. Han et al., "Millisecond-timescale optical control of neural dynamics in the nonhuman primate brain," *Neuron* **62**(2), 191–198 (2009).
64. X. Han et al., "A high-light sensitivity optical neural silencer: development and application to optogenetic control of non-human primate cortex," *Front. Syst. Neurosci.* **5**, 18 (2011).
65. J. Voigts et al., "The flexDrive: an ultra-light implant for optical control and highly parallel chronic recording of neuronal ensembles in freely moving mice," *Front. Syst. Neurosci.* **7**, 8 (2013).
66. J. Wang et al., "Integrated device for combined optical neuromodulation and electrical recording for chronic in vivo applications," *J. Neural Eng.* **9**(1), 016001 (2012).
67. I. Ozden et al., "A coaxial optrode as multifunction write-read probe for optogenetic studies in non-human primates," *J. Neurosci. Methods* **219**(1), 142–154 (2013).
68. E. Stark, T. Koos, and G. Buzsaki, "Diode probes for spatiotemporal optical control of multiple neurons in freely moving animals," *J. Neurophysiol.* **108**(1), 349–363 (2012).
69. O. Ruiz et al., "Optogenetics through windows on the brain in the nonhuman primate," *J. Neurophysiol.* **110**(6), 1455–1467 (2013).
70. A. N. Zorzos, E. S. Boyden, and C. G. Fonstad, "Multiwaveguide implantable probe for light delivery to sets of distributed brain targets," *Opt. Lett.* **35**(24), 4133–4135 (2010).
71. S. Royer et al., "Multi-array silicon probes with integrated optical fibers: light-assisted perturbation and recording of local neural circuits in the behaving animal," *Eur. J. Neurosci.* **31**(12), 2279–2291 (2010).
72. A. N. Zorzos et al., "Three-dimensional multiwaveguide probe array for light delivery to distributed brain circuits," *Opt. Lett.* **37**(23), 4841–4843 (2012).
73. H. Cao et al., "An integrated μLED optrode for optogenetic stimulation and electrical recording," *IEEE Trans. Biomed. Eng.* **PP**(99), 1 (2012).
74. T. I. Kim et al., "Injectable, cellular-scale optoelectronics with applications for wireless optogenetics," *Science* **340**(6129), 211–216 (2013).
75. J. P. Rickgauer and D. W. Tank, "Two-photon excitation of channelrhodopsin-2 at saturation," *Proc. Natl. Acad. Sci. U. S. A.* **106**(35), 15025–15030 (2009).
76. E. Papagiakoumou et al., "Scanless two-photon excitation of channelrhodopsin-2," *Nat. Methods* **7**(10), 848–854 (2010).
77. A. M. Packer, B. Roska, and M. Hausser, "Targeting neurons and photons for optogenetics," *Nat. Neurosci.* **16**(7), 805–815 (2013).
78. E. Papagiakoumou et al., "Functional patterned multiphoton excitation deep inside scattering tissue," *Nat. Photon.* **7**(4), 274–278 (2013).
79. B. K. Andrasfalvy et al., "Two-photon single-cell optogenetic control of neuronal activity by sculpted light," *Proc. Natl. Acad. Sci. U. S. A.* **107**(26), 11981–11986 (2010).
80. A. B. Arrenberg et al., "Optogenetic control of cardiac function," *Science* **330**(6006), 971–974 (2010).
81. T. Bruegmann et al., "Optogenetic control of heart muscle in vitro and in vivo," *Nat. Methods* **7**(11), 897–900 (2010).
82. O. J. Abilez, "Optogenetic LED array for perturbing cardiac electrophysiology," in *2013 35th Annual Int. Conf. of the IEEE Engineering in Medicine and Biology Society (EMBC)*, Osaka, IEEE (2013).
83. J. C. Williams et al., "Computational optogenetics: empirically-derived voltage- and light-sensitive channelrhodopsin-2 model," *PLoS Comput. Biol.* **9**(9), e1003220 (2013).
84. C. M. Ambrosi and E. Entcheva, "Optogenetic control of cardiomyocytes via viral delivery," *Methods Mol. Biol.* **1181**, 215–228 (2014).
85. Z. Jia et al., "Stimulating cardiac muscle by light: cardiac optogenetics by cell delivery," *Circ. Arrhythm. Electrophysiol.* **4**(5), 753–760 (2011).
86. O. J. Abilez et al., "Multiscale computational models for optogenetic control of cardiac function," *Biophys. J.* **101**(6), 1326–1334 (2011).
87. J. Wong, O. J. Abilez, and E. Kuhl, "Computational optogenetics: a novel continuum framework for the photoelectrochemistry of living systems," *J. Mech. Phys. Solids* **60**(6), 1158–1178 (2012).
88. F. Helmchen et al., "A miniature head-mounted two-photon microscope. high-resolution brain imaging in freely moving animals," *Neuron* **31**(6), 903–912 (2001).
89. H. Bao et al., "Fast handheld two-photon fluorescence microendoscope with a 475 μm $\times$ 475 μm field of view for in vivo imaging," *Opt. Lett.* **33**(12), 1333–1335 (2008).
90. Y. Zhao, H. Nakamura, and R. J. Gordon, "Development of a versatile two-photon endoscope for biological imaging," *Biomed. Opt. Express* **1**(4), 1159–1172 (2010).
91. C. P. Lin and R. H. Webb, "Fiber-coupled multiplexed confocal microscope," *Opt. Lett.* **25**(13), 954–956 (2000).
92. D. Bird and M. Gu, "Compact two-photon fluorescence microscope based on a single-mode fiber coupler," *Opt. Lett.* **27**(12), 1031–1033 (2002).
93. R. P. Barretto and M. J. Schnitzer, "In vivo optical microendoscopy for imaging cells lying deep within live tissue," *Cold Spring Harb. Protoc.* **2012**(10), 1029–1034 (2012).
94. J. C. Jung et al., "In vivo mammalian brain Imaging using one- and two-photon fluorescence microendoscopy," *J. Neurophysiol.* **92**(5), 3121–3133 (2004).
95. J. C. Jung and M. J. Schnitzer, "Multiphoton endoscopy," *Opt. Lett.* **28**(11), 902–904 (2003).
96. S. Y. Leigh and J. T. Liu, "Multi-color miniature dual-axis confocal microscope for point-of-care pathology," *Opt. Lett.* **37**(12), 2430–2432 (2012).
97. J. Knittel et al., "Endoscope-compatible confocal microscope using a gradient index-lens system," *Opt. Commun.* **188**(5–6), 267–273 (2001).
98. W. Göbel et al., "Miniaturized two-photon microscope based on a flexible coherent fiberbundle and a gradient-index lens objective," *Opt. Lett.* **29**(21), 2521–2523 (2004).

99. K. K. Ghosh et al., "Miniaturized integration of a fluorescence microscope," *Nat. Methods* **8**(10), 871–878 (2011).
100. M. E. Llewellyn et al., "Minimally invasive high-speed imaging of sarcomere contractile dynamics in mice and humans," *Nature* **454**(7205), 784–788 (2008).
101. D. R. Rivera et al., "Use of a lensed fiber for a large-field-of-view, high-resolution, fiber-scanning microendoscope," *Opt. Lett.* **37**(5), 881–883 (2012).
102. B. A. Flusberg et al., "High-speed, miniaturized fluorescence microscopy in freely moving mice," *Nat. Methods* **5**(11), 935–938 (2008).
103. J. T. Liu et al., "Micromirror-scanned dual-axis confocal microscope utilizing a gradient-index relay lens for image guidance during brain surgery," *J. Biomed. Opt.* **15**(2), 026029 (2010).
104. B. A. Flusberg et al., "In vivo brain imaging using a portable 3.9 gram two-photon fluorescence microendoscope," *Opt. Lett.* **30**(17), 2272–2274 (2005).
105. W. Piyawattanametha et al., "In vivo brain imaging using a portable 2.9 g two-photon microscope based on a microelectromechanical systems scanning mirror," *Opt. Lett.* **34**(15), 2309–2311 (2009).
106. Y. Honda and P. J. Fitzgerald, "Frontiers in intravascular imaging technologies," *Circulation* **117**(15), 2024–2037 (2008).
107. H. G. Bezerra et al., "Intracoronary optical coherence tomography: a comprehensive review clinical and research applications," *JACC Cardiovasc. Interv.* **2**(11), 1035–1046 (2009).
108. D. S. Baim and W. Grossman, *Grossman's Cardiac Catheterization, Angiography, and Intervention*, 7th ed., Lippincott Williams & Wilkins, Philadelphia, PA (2006).
109. R. D. Madder, D. H. Steinberg, and R. D. Anderson, "Multimodality direct coronary imaging with combined near-infrared spectroscopy and intravascular ultrasound: initial US experience," *Catheter. Cardiovasc. Interv.* **81**(3), 551–557 (2013).
110. C. M. Ambrosi et al., "Virtual histology of the human heart using optical coherence tomography," *J. Biomed. Opt.* **14**(5), 054002 (2009).
111. G. M. London et al., "Brachial artery diameter changes associated with cardiopulmonary baroreflex activation in humans," *Am. J. Physiol.* **258**(3 Pt 2), H773–H777 (1990).
112. G. Schnyder et al., "Common femoral artery anatomy is influenced by demographics and comorbidity: implications for cardiac and peripheral invasive studies," *Catheter. Cardiovasc. Interv.* **53**(3), 289–295 (2001).
113. D. Tartiere et al., "Estimation of the diameter and cross-sectional area of the internal jugular veins in adult patients," *Crit. Care* **13**(6), R197 (2009).
114. A. Fronek et al., "Common femoral vein dimensions and hemodynamics including Valsalva response as a function of sex, age, and ethnicity in a population study," *J. Vasc. Surg.* **33**(5), 1050–1056 (2001).
115. C. J. Davidson and R. O. Bonow, "Cardiac Catheterization," in *Heart Disease. A Textbook of Cardiovascular Medicine*, 5th ed., E. B. Braunwald, Ed., pp. 177–203, WB Saunders, Philadelphia, PA (1997).
116. C. Landau, R. A. Lange, and L. D. Hillis, "Percutaneous transluminal coronary angioplasty," *N. Engl. J. Med.* **330**(14), 981–993 (1994).
117. J. T. Dodge, Jr. et al., "Lumen diameter of normal human coronary arteries. Influence of age, sex, anatomic variation, and left ventricular hypertrophy or dilation," *Circulation* **86**(1), 232–246 (1992).
118. I. Singer, *Interventional Electrophysiology*, Williams & Wilkins, Baltimore, MD (1997).
119. D. F. Guthaner, L. Wexler, and G. Harell, "CT demonstration of cardiac structures," *AJR Am. J. Roentgenol.* **133**(1), 75–81 (1979).
120. A. Habib et al., "The anatomy of the coronary sinus venous system for the cardiac electrophysiologist," *Europace* **11**(Suppl 5), v15–v21 (2009).
121. B. Genc et al., "Assessment of the coronary venous system by using cardiac CT," *Diagn. Interv. Radiol.* **19**(4), 286–293 (2013).
122. M. Mesradi et al., "Experimental and analytical comparative study of optical coefficient of fresh and frozen rat tissues," *J. Biomed. Opt.* **18**(11), 117010 (2013).
123. A. Roggan et al., "Optical properties of circulating human blood in the wavelength range 400–2500 nm," *J. Biomed. Opt.* **4**(1), 36–46 (1999).
124. J. P. Holt et al., "Geometric similarity of aorta, venae cavae, and certain of their branches in mammals," *Am. J. Physiol.* **241**(1), R100–R104 (1981).
125. G. B. West, J. H. Brown, and B. J. Enquist, "A general model for the origin of allometric scaling laws in biology," *Science* **276**(5309), 122–126 (1997).
126. I. Singer and J. Kupersmith, *Clinical Manual of Electrophysiology*, Williams & Wilkins, Baltimore, MD (1993).
127. S. Rohr and B. M. Salzberg, "Multiple site optical recording of transmembrane voltage (MSORTV) in patterned growth heart cell cultures: assessing electrical behavior, with microsecond resolution, on a cellular and subcellular scale," *Biophys. J.* **67**(3), 1301–1315 (1994).
128. G. Kanaporis et al., "Optical mapping at increased illumination intensities," *J. Biomed. Opt.* **17**(9), 096007 (2012).
129. A. Matiukas et al., "New near-infrared optical probes of cardiac electrical activity," *Am. J. Physiol. Heart Circ. Physiol.* **290**(6), H2633–H2643 (2006).
130. L. M. Loew, "Characterization of potentiometric membrane dyes," in *Biomembrane Electrochemistry*, Chapter 8, pp. 151–173, American Chemical Society, Washington, DC (1994).
131. A. Matiukas et al., "Near-infrared voltage-sensitive fluorescent dyes optimized for optical mapping in blood-perfused myocardium," *Heart Rhythm* **4**(11), 1441–1451 (2007).
132. H. Mutoh and T. Knopfel, "Probing neuronal activities with genetically encoded optical indicators: from a historical to a forward-looking perspective," *Pflugers Arch.* **465**(3), 361–371 (2013).
133. D. Maclaurin et al., "Mechanism of voltage-sensitive fluorescence in a microbial rhodopsin," *Proc. Natl. Acad. Sci. U. S. A.* **110**(15), 5939–5944 (2013).
134. J. H. Hou, V. Venkatachalam, and A. E. Cohen, "Temporal dynamics of microbial rhodopsin fluorescence reports absolute membrane voltage," *Biophys. J.* **106**(3), 639–648 (2014).
135. J. M. Kralj et al., "Optical recording of action potentials in mammalian neurons using a microbial rhodopsin," *Nat. Methods* **9**(1), 90–U130 (2011).
136. Y. Gong, J. Z. Li, and M. J. Schnitzer, "Enhanced archaerhodopsin fluorescent protein voltage indicators," *PLoS One* **8**(6), e66959 (2013).
137. C. M. Ambrosi et al., "Cardiac applications of optogenetics," in *Prog. Biophys. Mol. Biol.* (in press) (2014).
138. C. Bamann et al., "Spectral characteristics of the photocycle of channelrhodopsin-2 and its implication for channel function," *J. Mol. Biol.* **375**(3), 686–694 (2008).
139. Z. V. Guo, A. C. Hart, and S. Ramanathan, "Optical interrogation of neural circuits in Caenorhabditis elegans," *Nat. Methods* **6**(12), 891–896 (2009).
140. B. A. Flusberg et al., "Fiber-optic fluorescence imaging," *Nat. Methods* **2**(12), 941–950 (2005).
141. P. M. Delaney, M. R. Harris, and R. G. King, "Fiber-optic laser scanning confocal microscope suitable for fluorescence imaging," *Appl. Opt.* **33**(4), 573–577 (1994).
142. F. Helmchen, "Miniaturization of fluorescence microscopes using fibre optics," *Exp. Physiol.* **87**(6), 737–745 (2002).
143. D. H. Kim et al., "Flexible and stretchable electronics for biointegrated devices," *Annu. Rev. Biomed. Eng.* **14**, 113–128 (2012).
144. P. Lee et al., "Simultaneous voltage and calcium mapping of genetically purified human induced pluripotent stem cell-derived cardiac myocyte monolayers," *Circ. Res.* **110**(12), 1556–1563 (2012).

Aleksandra Klimas is a PhD candidate in biomedical engineering at Stony Brook University. She received her BSE degree in electrical and computer engineering and completed the requirements for a BS degree in physics from Duke University in 2009 and received her MS degree in optics from the University of Rochester in 2011. Her current research interests include optical solutions for cardiac optogenetics applications.

Emilia Entcheva is a professor of biomedical engineering at Stony Brook University with joint appointments in physiology and biophysics and cardiology. She holds a PhD degree in biomedical engineering from the University of Memphis and BS/MS degrees in electrical engineering from Technical University in Sofia, Bulgaria. After a postdoctoral fellowship at Johns Hopkins University, she started her own laboratory at Stony Brook in 2001. Her research group has contributed to the development of new tools for optical mapping of excitation in cardiac cells, computational modeling of cardiac electrophysiology, and recently has spearheaded efforts in cardiac optogenetics.